Electronic Supplementary Material (ESI) for ChemComm.

Supporting Information

Ultrasonic reduction: An unconventional route to exsolute Ag from perovskite La(Ag)$FeO_{3-\delta}$ for enhanced catalytic oxidation activity

Haijun Wu, Zhibin Geng*, Xu Zhao, Ming Ya, Taotao Huang, Junzhi Li, Liping Li, and Guangshe Li*

State Key Laboratory of Inorganic Synthesis and Preparative Chemistry, College of Chemistry, Jilin University, Changchun 130012, P. R. China

* Corresponding Author Zhibin Geng; Email: gengzb@jlu.edu.cn

* Corresponding Author Liping Li; Email: lipingli@jlu.edu.cn

* Corresponding Author Guangshe Li; Email: guangshe@jlu.edu.cn

Catalyst preparation

Preparation of $La_{0.9}FeO_{3-\delta}$

The catalyst $La_{0.9}FeO_{3-\delta}$ was prepared by sol-gel method. The preparation process is as follows: 4.5 mmol La $(NO_3)_3 \cdot 6H_2O$, 5 mmol Fe $(NO_3)_3 \cdot 9H_2O$ are added to 5 ml deionized water, and citric acid and ethylene glycol are added in proportion to metal ions: citric acid: ethylene glycol = 1:1.5: 3. After stirring for 1h, steam the excess water in a water bath at 80 ℃, and put the obtained gel into a 170 ℃ oven to dry and foam for 8 h. The obtained precursor was ground and calcined in Muffle furnace at 600 ℃ for 2 h at a heating rate of 10 ℃·min^{-1}, the final product $La_{0.9}FeO_{3-\delta}$ named LFO.

Preparation of $La_{0.87}Ag_{0.03}FeO_{3-\delta}$

4.35 mmol La $(NO_3)_3 \cdot 6H_2O$,5 mmol Fe $(NO_3)_3 \cdot 9H_2O$, 0.15 mmol $AgNO_3$ are added to 5 ml deionized water, and other steps are the same as that of $La_{0.9}FeO_{3-\delta,}$ and named it LAFO.

Preparation of $La_{0.87}Ag_{0.03}FeO_{3-\delta}$ after ultrasonic reduction

LAFO (0.2 g) was uniformly dispersed in 50 ml deionized water, and 3 g of $NaBH_4$ was dissolved in 20 ml deionized water. The power and time of the ultrasonic machine were adjusted to 10% and 1min. It was poured into the catalyst aqueous solution for ultrasonic treatment when $NaBH_4$ solution no longer had bubbles. After the ultrasonic reduction treatment, the solution was drained, washed, and freeze-dried, the catalyst after ultrasonic reduction was named LAFO-UR. The ultrasonic instrument used is the non-contact ultrasonic cell crusher (SCIENTZ08-IIIC) produced by Ningbo Xinzhi Biotechnology LTD with a maximum ultrasonic power of 1800 W.

Characterization of catalyst

The X-ray diffraction (**XRD**) pattern of the powder was recorded by Cu Kα radiation (λ = 1.5418 A) using Rigaku's D/Max-2550 X-ray diffractometer. At the room temperature of 50 kV and 200 mA, the scanning speed is step8s, and the scanning Angle range is 10°≤2θ≤80°;

The Transmission electron microscopy (**TEM**) images were recorded by Tecnai G2 S-Twin F20 (FEI Corporation);

The **Raman** spectra were recorded at 532 nm by inVia (Renishaw Company) at λ = 532 nm;

The Fourier Transform infrared spectroscopy (**FT-IR**) was detected under vacuum conditions by VERTEX 80V(Bruker);

The X-ray photoelectron spectroscopy (**XPS**) was recorded with the ESCALAB 250 electron spectrometer (Thermo Fisher Scientific), with Al Kα (1486.6 eV) as the X-ray excitation source. Nitrogen adsorption-desorption measurements were taken on the Micromeritics 2020 analyzer (Micromeritics Instruments Corporation); The sample was first degassed at 200 °C under vacuum and then measured at 77.35 K;

The X-ray absorption spectra (**XAS**) of the Fe l side and O k side were measured on the BL12B-a beam line of the National Synchrotron Radiation Laboratory (NSRL) of the University of Science and Technology of China. The spectra are collected in a total electron yield mode under vacuum conditions above 5×10^{-8} Pa. At the Shanghai Synchrotron Radiation Facility (SSRF), Fe K-edge spectra in the range of 6910 ~ 7910 eV were collected at room temperature in transmission mode. The radiation was monochromized with Si (111) channel cutting monochromator, and the energy value of the sample was calibrated with standard iron foil; Ag-K-edge was obtained on the beamlines MCD-A and MCD-B (Soochow Beamline for Energy Materials) at NSRL;

The programmed temperature reduction of H_2 (**H_2-TPR**) was measured on the Micromeritics AutoChem II 2920 instrument. About 30 mg of the sample was heated from 30 °C to 900 °C at 10 °C·min^{-1} in a 10% H_2/Ar gas mixture (30 mL·min^{-1}); Temperature-programmed desorption of O2 (O2-TPD) was performed using the same

apparatus. Approximately 30 mg of the samples was pretreated in an Ar flow at 200 °C for 2 h and cooled to 50 °C in an O2 atmosphere for 1 h, and then physically adsorbed gases were removed in the pure He atmosphere for 1 h. The O2-TPD signal was finally acquired from 50 to 900 °C at 10 °C·min–1 with O2 desorption.

The in situ diffuse reflection Fourier transform infrared spectroscopy (**DRIFTS**) analysis is performed on a Nicolet iS50 Fourier transform infrared spectrometer. Prior to measurement, the sample (15 mg) was purged with pure N_2 at room temperature at a flow rate of 20 mL·min^{-1} for 30 minutes to remove contaminants, and then background spectra were collected for spectral correction. The reaction gas is then introduced into the in-situ chamber at a flow rate of 19.6 mL·min^{-1}. In order to obtain the required spectrum, an average of 48 scans are performed each time;

The Thermogravimetric Mass Spectrometry (**TG-MS**) was measured on the NETZSCH STA449F3 QMS403D \ Bruker V70 instrument, about 20 mg of the sample was heated from 30 °C to 650 °C at 10 °C·min^{-1} in a N_2 gas atmosphere.

Performance test

The sample (50 mg) was placed in a fixed-bed quartz reactor with a flow rate of 19.6mL· min^{-1} for the reaction gas (1%CO/ 20%O_2/He). The catalytic activity of the sample was determined by heating at a fixed rate in the temperature range of 20 - 400 °C for 10 min at each test temperature point to establish stable measurements. CO concentration was analyzed by Shimadzu GC-2014C gas chromatography with thermal conductivity detector. The CO conversion rate is calculated by dividing the difference before and after the CO conversion by the total amount before the CO conversion.

The calculation of the amount of inserted protons

The probable amount of inserted protons could be calculated by TG data. As the actual existence form of H in the lattice is O-H, the mass loss of LAFO-UR at 600 °C is 1% higher than that of LAFO due to the existence and losses of O-H. The calculation process is as follows:

$$\omega_H = \omega_{OH}\frac{M_H}{M_{OH}} = \frac{y \times M_H}{M_{LAFO-UR}}$$

Where ω_H is the mass fraction of H in LAFO-UR. ω_{OH} is the mass fraction of O-H in LAFO-UR. M_H is the molar mass of H, M_{OH} is the molar mass of O-H, $M_{LAFO-UR}$ (approximately equal to 228) is the molar mass of $Ag_{0.03-x}/La_{0.87}Ag_xH_yFeO_{3-\delta}$, y is the moles of protons inserted in the unit mass of LAFO-UR.

According to TG-MS data, ω_{OH}=1%, thus we can calculate that y=0.13.

Calculation of activation energy

The reaction rate of the samples was calculated by the following formula

$$k(mol\cdot s^{-1}\cdot g_{cat}^{-1}) = \frac{\alpha_{co}(\%) \times 1\% \times V(cm^3\cdot min^{-1})}{22.4 \times 60 \times 1000 \times m(g)}$$

where V is the total gas flow rate (19.6 $cm^3 \cdot min^{-1}$) and m is the mass (0.05 g) of the examined sample. To better evaluate the catalytic activity, the apparent activation energy was calculated using the classical Arrhenius formula.

$$k = k_0 e^{-E_a/RT}$$

Derived from the above formula

$$-ln\left(\frac{\alpha_{co}(\%) \times 1\% \times 19.6(cm^3\cdot min^{-1})}{22.4 \times 60 \times 1000 \times 0.05(g)}\right) = E_a/RT,$$

Given the conversion rate of CO at different temperatures, the relationship graph between - ln (k) and 1/T can be obtained. The energy barrier, Ea ($kJ\cdot mol^{-1}$), was obtained from the slope (E_a/R) of −ln (k) versus 1/T.

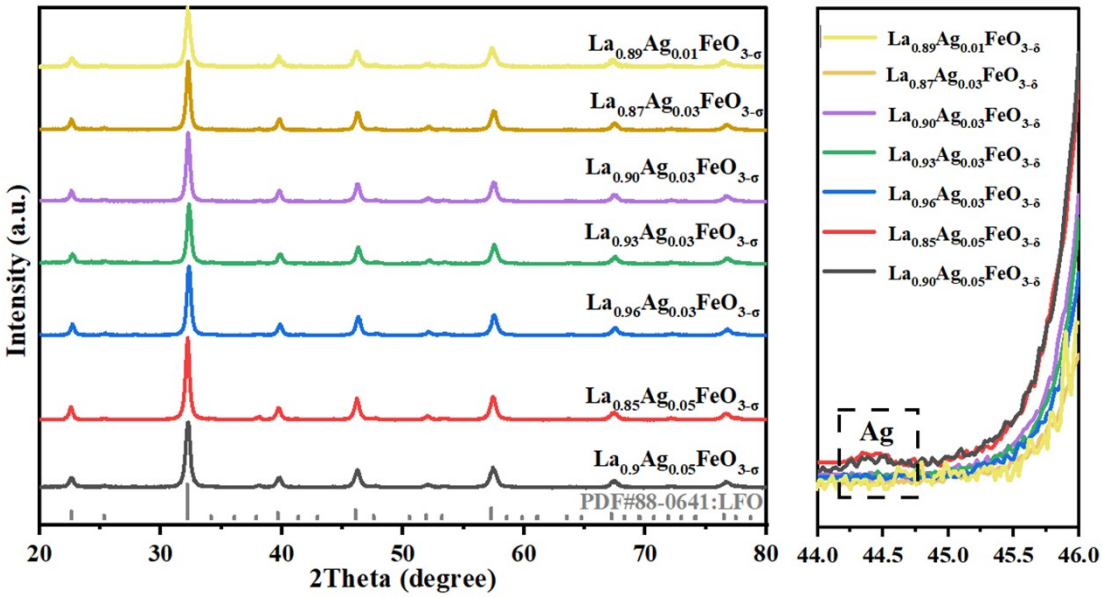

Figure S1. XRD patterns of the LAFO

Figure S1 shows the LAFO with different doping amounts of Ag and different A-site defects. When the doping amount of Ag is 5%, the peak position of Ag is shown at $2\theta = 44.5°$, and the doping amount of Ag is 1%, which is lower than the detection limit of many instruments, and the doping amount of Ag is determined to be 3%.

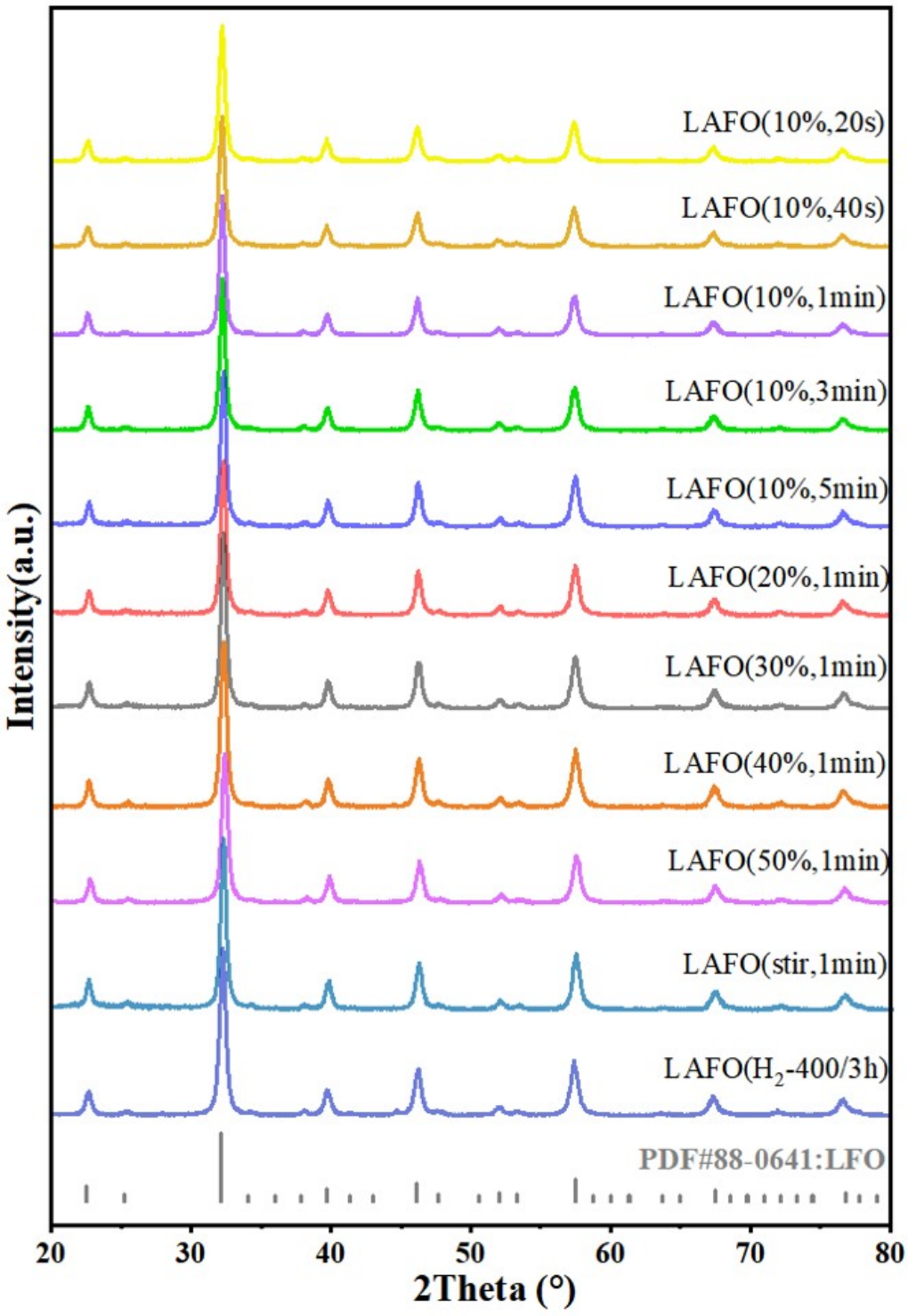

Figure S2. A series of XRD of LAFO-UR under different reaction conditions.

After LAFO reduction treatment at different times and powers, there is no significant difference in crystal structure.

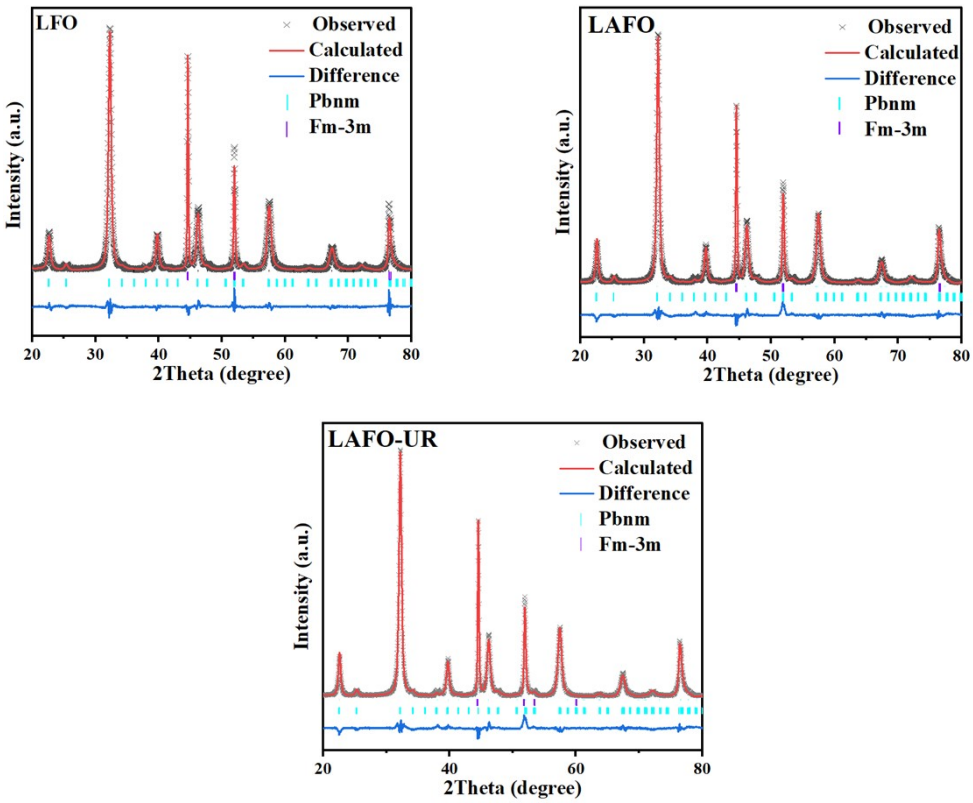

Figure S3. XRD refined patterns of LFO, LAFO, and LAFO-UR.

Sample	lattice parameter (A)				Refinement factors		
	a	b	c	V	χ^2	R_{Wp}	R_p
LFO	5.568	5.567	7.863	243.73	4.52	0.112	0.0721
LAFO	5.565	5.588	7.905	245.82	3.29	0.0771	0.0554
LAFO-UR	5.57	5.573	7.883	244.7	3.735	0.086	0.0598

Table S1.Lattice parameters, XRD refinement fctors of LFO, LAFO, and LAFO-UR.

The lattice parameters and cell volume of LAFO both increase compared with LFO, this is due to lattice expansion caused by Ag^+ radius being larger than La^{3+} radius. Compared with LAFO, the lattice parameters and cell volume of LAFO-UR decrease due to the dissolution of Ag in the lattice, which leads to a lattice shrinkage.

Sample	Concentration		
	La	Ag	Fe
LFO	49.19	--	22.36
LAFO	45.11	1.241	21.08
LAFO-UR	42.51	1.024	19.77

Table S2. ICP-OES results of LFO, LAFO, and LAFO-UR.

The ratio between La, Ag, and Fe can be obtained from ICP results, and the chemical formula of the obtained sample can be determined as $La_{0.9}FeO_{3-\delta}$, $La_{0.87}Ag_{0.03}FeO_{3-\delta}$ and $Ag/La_{0.87}Ag_xFeO_{3-\delta}$, which is consistent with the results of SEM-EDS below.

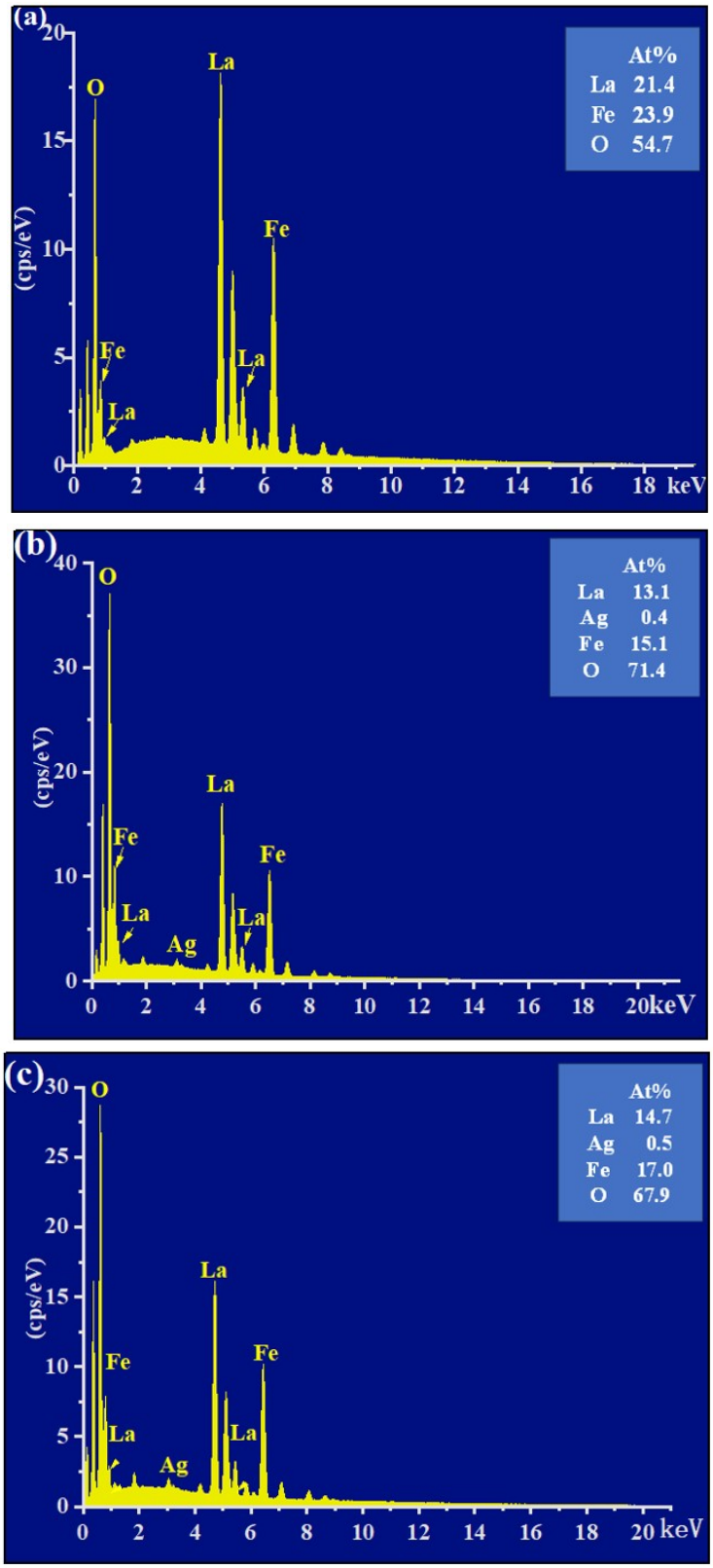

Figure S4. SEM-EDS results of (a) LFO, (b) LAFO, and (c) LAFO-UR.

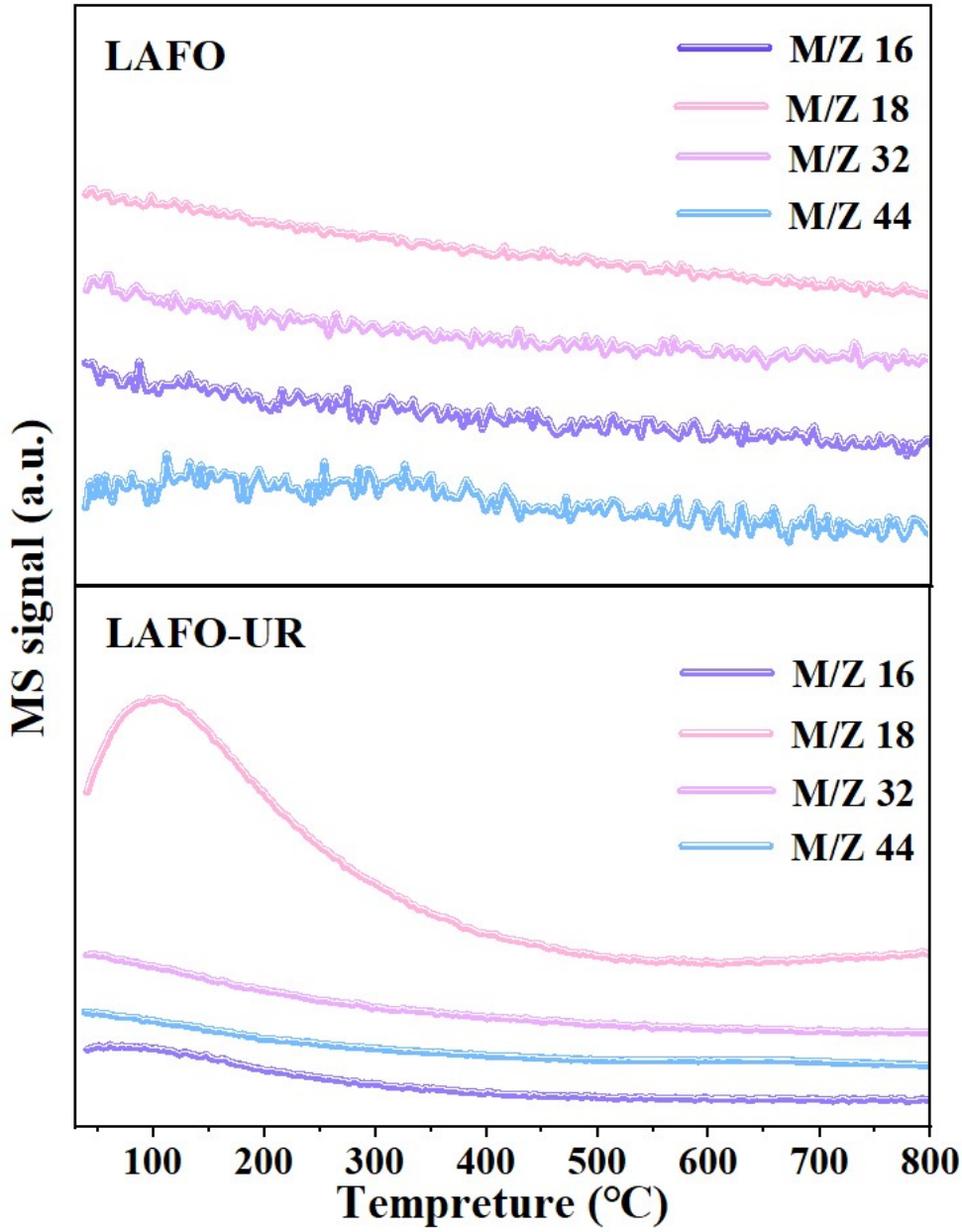

Figure S5.TG-MS of LAFO and LAFO-UR.

The weight loss of LAFO-UR is more than that of LAFO due to hydrogen ions combined with lattice oxygen after LAFO ultrasonic reduction and escape in form of water.

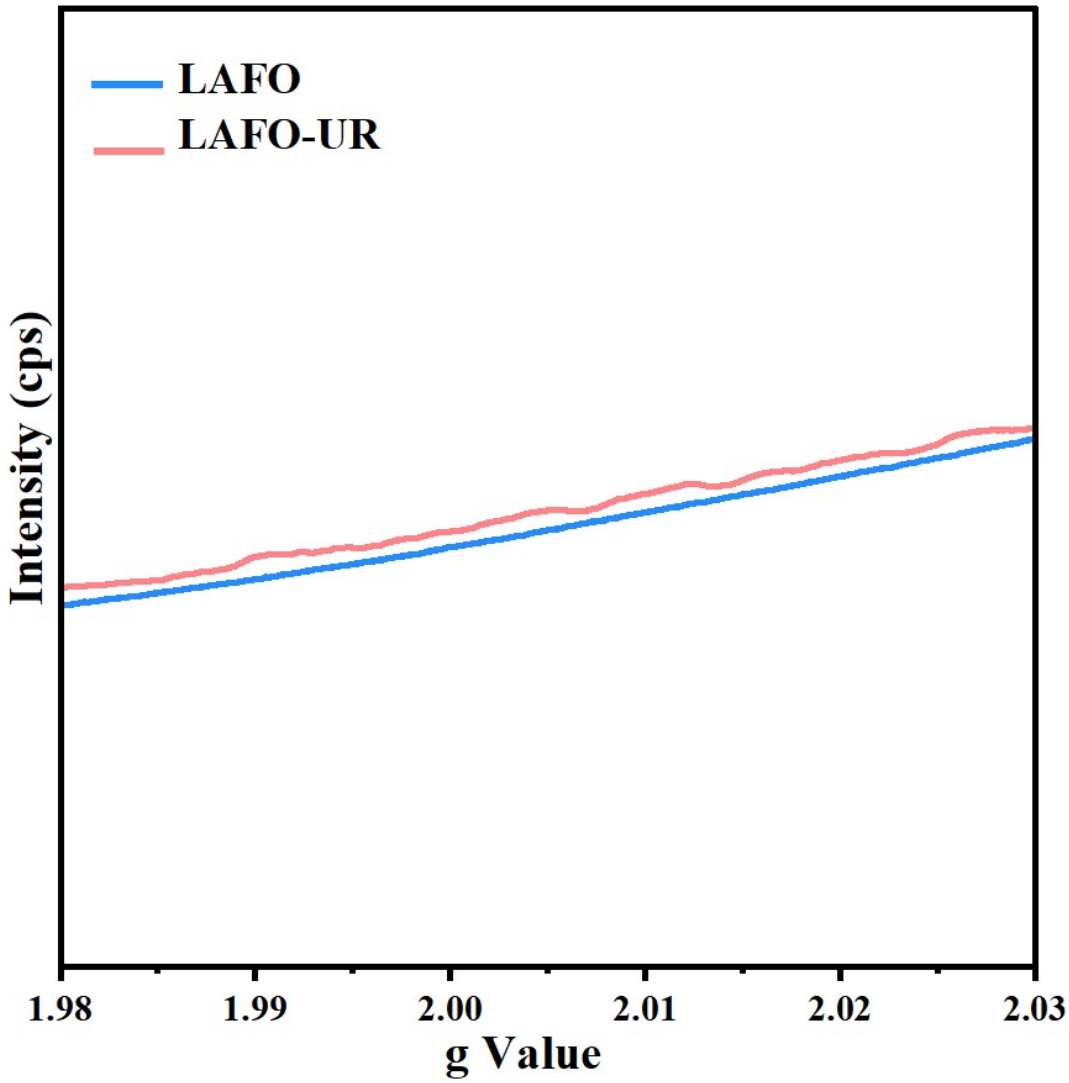

Figure S6. EPR spectra of LAFO, LAFO-UR catalysts.

LAFO did not produce oxygen vacancies after ultrasonic reduction treatment.

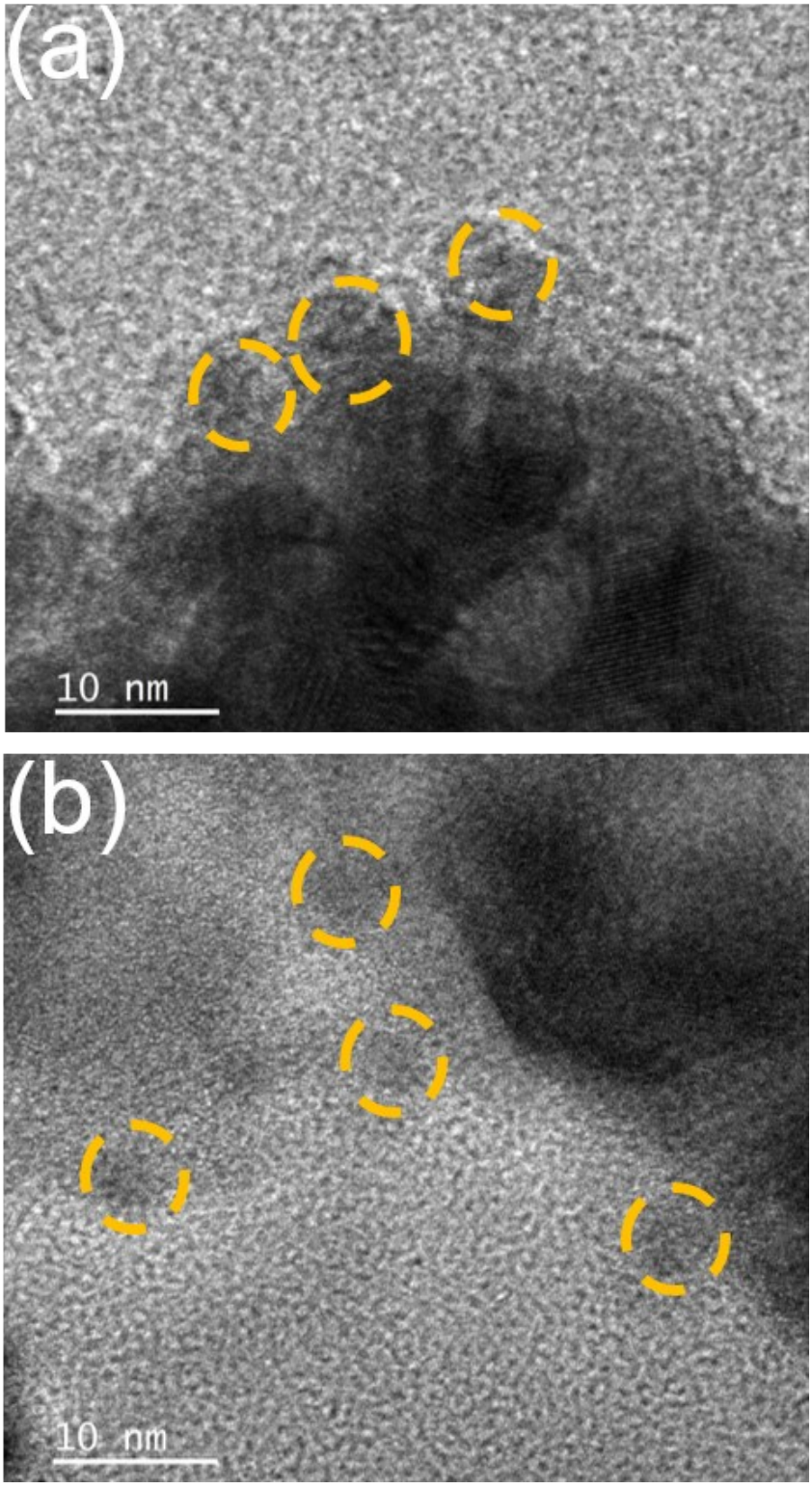

Figure S7. HRTEM of elemental Ag on the surface of LAFO-UR.

The yellow circle represents elemental Ag.

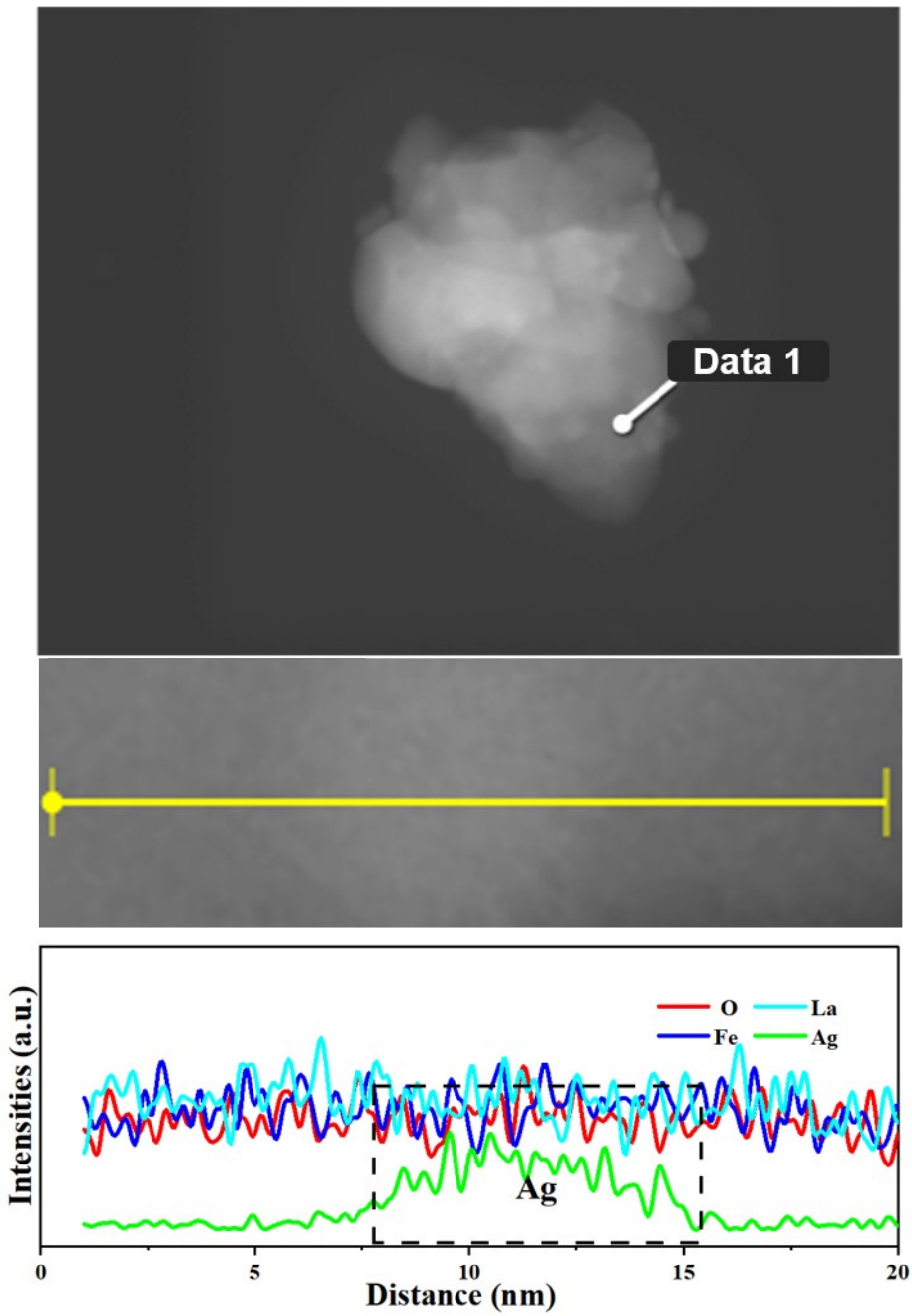

Figure S8. Linear scan of LAFO-UR.

The Ag shows aggregated distribution, and the surface nanoparticle is mainly consist of Ag element.

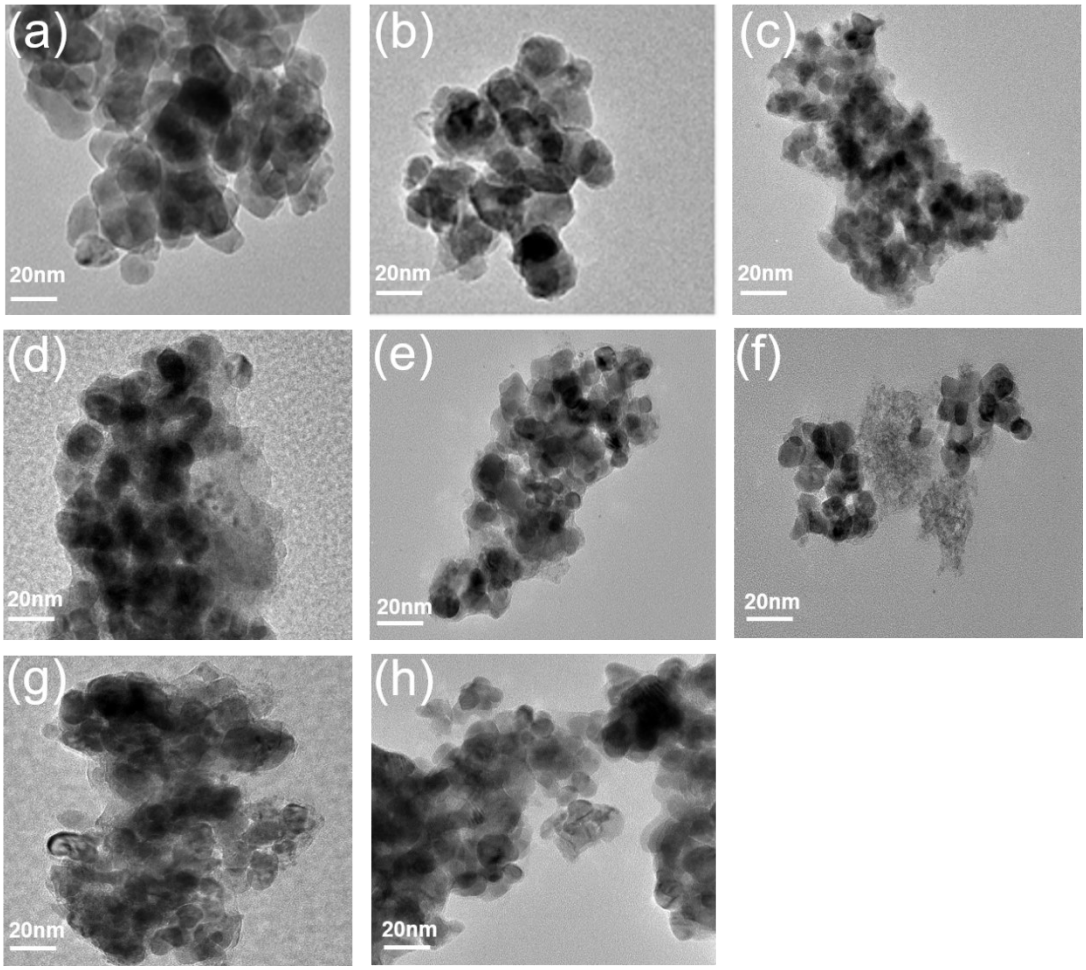

Figure S9. TEM images of LAFO-UR were obtained under the condition of ultrasound time of 1min and ultrasound power of (a) 0%, (b) 10%, (c) 20%, (d) 30%, (e) 40%, (f) 50%, (g) stirring at 1min, (h) LAFO-H_2-400.

With the increase of ultrasonic power, the structural collapse of LAFO is gradually serious. resulting in a sheet structure covered the surface of the particles, which may be the formation of hydroxyl oxides [1].

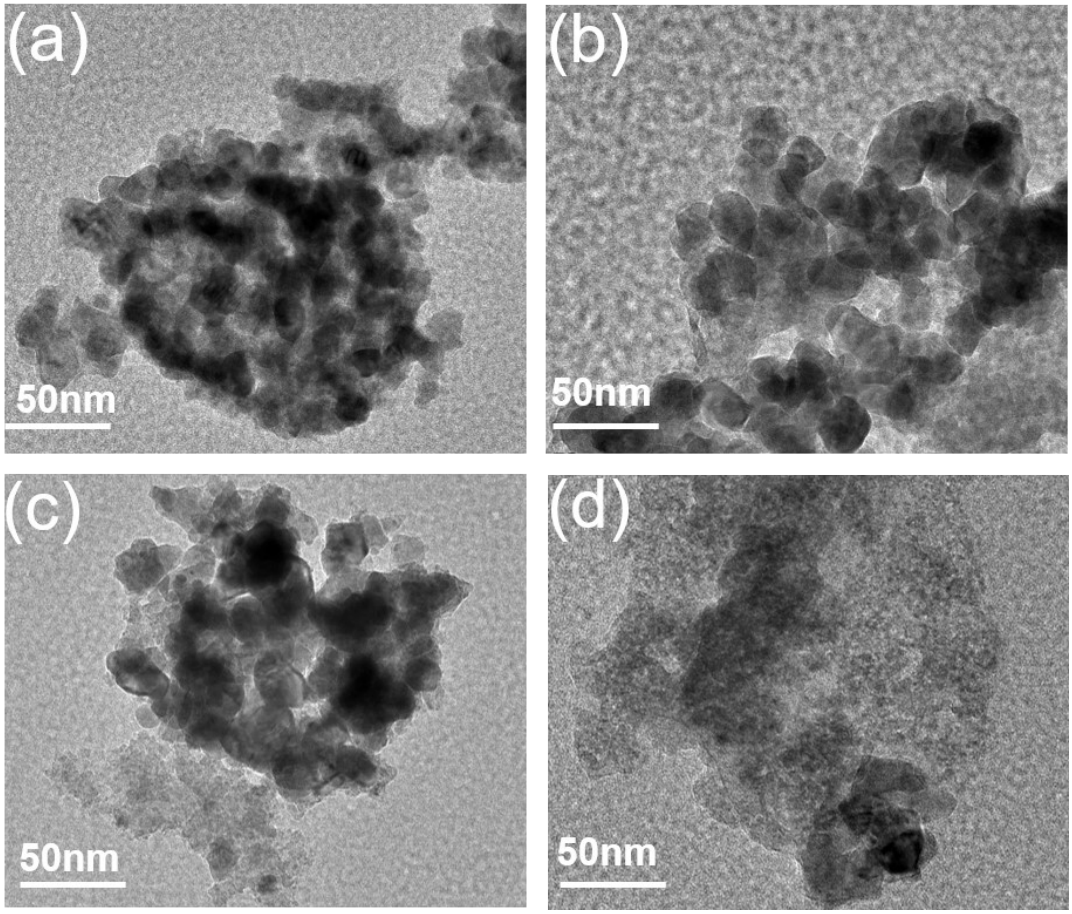

Figure S10. TEM images of catalysts LAFO-UR were obtained under the condition of ultrasound power of 10% and ultrasound time of (a) 20s, (b) 40s, (c) 3min, (d) 5min.

High ultrasonic power (Fig. S7) and too long ultrasonic time (Fig. S8) had a great impact on the morphology of the catalyst, resulting in a sheet structure covered the surface of the particles, which may be the formation of hydroxyl oxides [1].

Electrocatalysts	Fe-O-Fe	Other oxygen species (Fe-O-H, etc.)
LFO	55.87%	44.18%
LAFO	55.56%	44.44%
LAFO-UR	31.03%	68.97%

Table S3. O 1s XPS peak deconvolution results.

After ultrasonic reduction, a large amount of lattice oxygen (Fe-O-Fe) is converted to Fe-O-H.

Fe L-edge	LAFO	LAFO-UR
Intensity of Peak a	4.01	3.29
Intensity of Peak b	8.57	6.72
Intensity ratio: I_b/I_a	2.13	2.04

Table S4. Fe L-edge data of LFO, LAFO, and LAFO-UR.

O L-edge	LAFO	LAFO-UR
Intensity of Peak a	1.18	0.88
Intensity of Peak b	1.26	0.98
Intensity ratio: I_b/I_a	1.07	1.11

Table S5. O K-edge data of LFO, LAFO, and LAFO-UR.

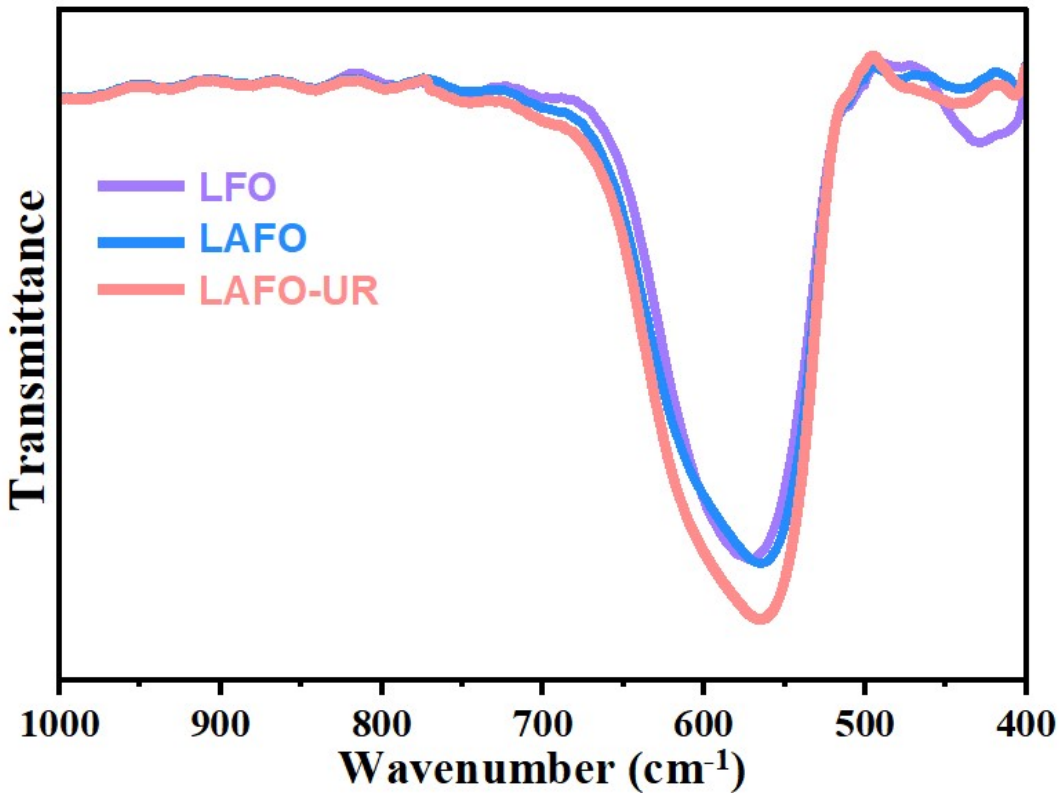

Figure S11. FT-IR spectroscopy of the LFO, LAFO, and LAFO-UR.

In the 400-1000 cm^{-1} range, peak 1 at 440 cm^{-1} can be observed to be attributed to the bending vibration of O-Fe-O in the FeO_6 octahedron, while peak 2 at 560 cm^{-1} is associated with the tensile vibration of Fe-O. The band at 427 cm^{-1} can be attributed to the O-Fe-O deformation vibration in LFO (v2 mode). The same bands in LAFO and LAFO-UR are located at 437 $cm^{-1}$and 441 cm^{-1}, which are shifted towards higher wavenumbers due to the interaction of Ag and LFO. The displacement of LAFO-UR is larger than that of LAFO, which can be attributed to the alteration of the coordination environment caused by Ag doping, after LAFO reduction, because the exsolution of elemental Ag shows a stronger interaction than LAFO [2].

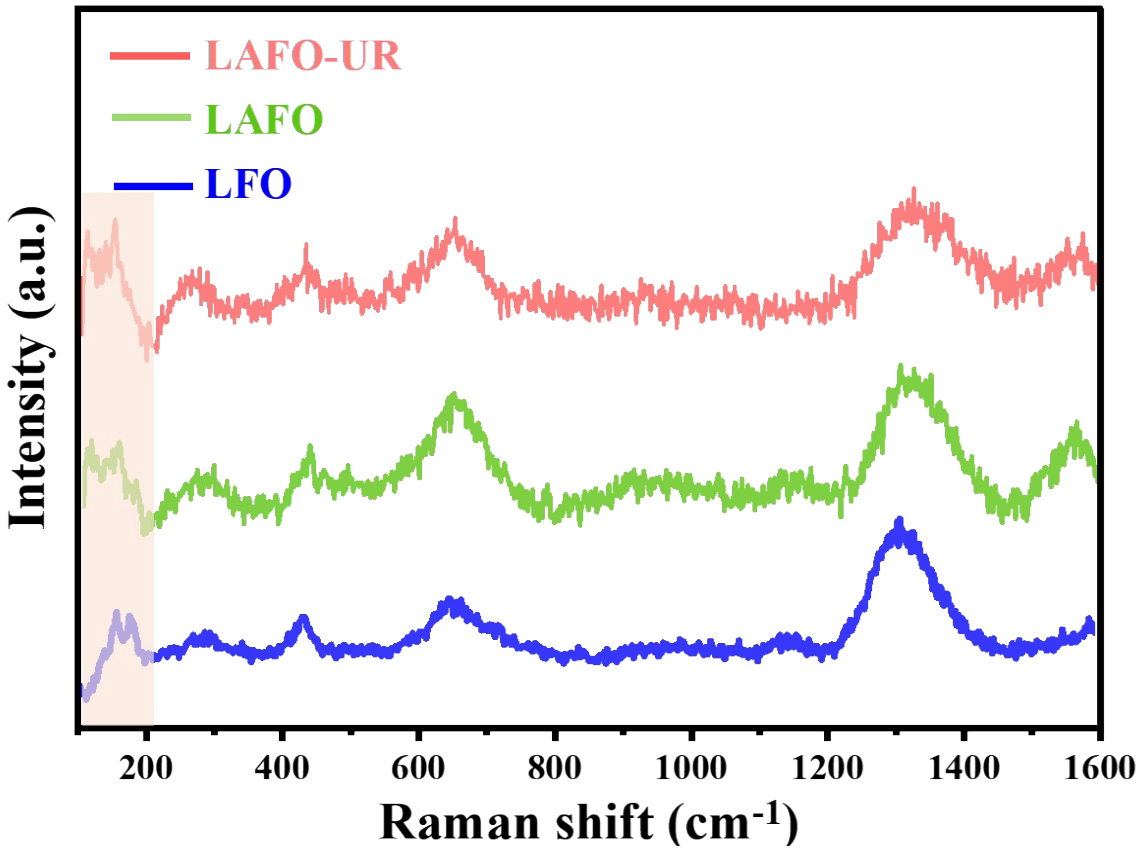

Figure S12. Raman spectra of LFO, LAFO, and LAFO-UR.

The bands at 286 cm^{-1} and 430 cm^{-1} are related to the curvature of FeO_6, the bands at 650 cm^{-1} are related to the stretching of Fe−O bonds, the bands at 1135 cm^{-1} belong to monophoton scattering, and the band at 1312 cm^{-1} belongs to diphoton scattering. In the 156 $cm^{-1}$and 175 cm^{-1} bands related to La motion, due to the interaction of Ag and LFO, a blue shift can be observed in LAFO (113 cm^{-1} and 154 cm^{-1}) and LAFO-UR (113 $cm^{-1}$and 150 cm^{-1}), the displacement of LAFO-UR is large [2].

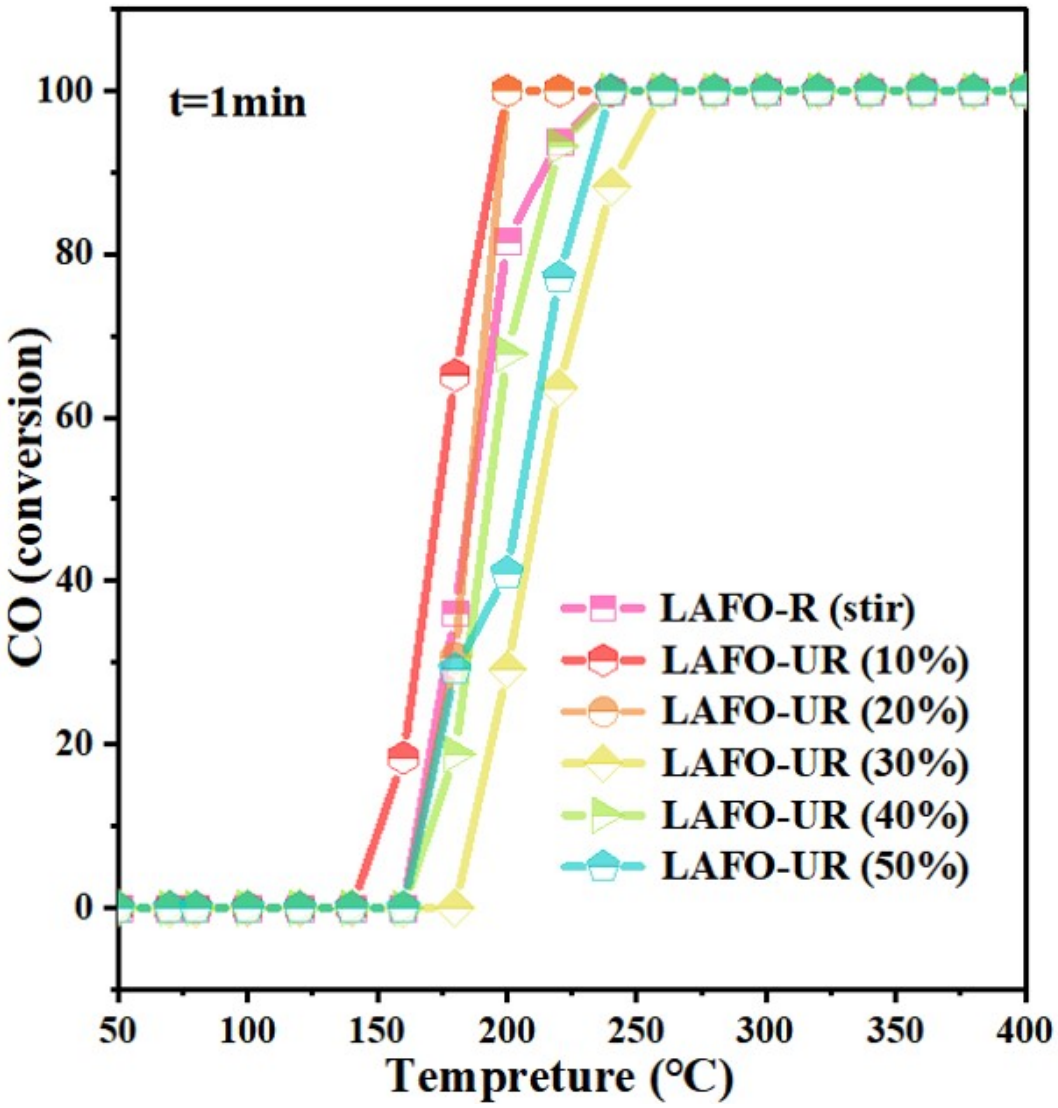

Figure S13. Light-off curves for CO oxidation of LAFO at different ultrasonic powers.

The figure shows the CO catalytic oxidation capacity of LAFO at different ultrasonic powers (t=1min), LAFO catalytic capacity being the best at 10% power.

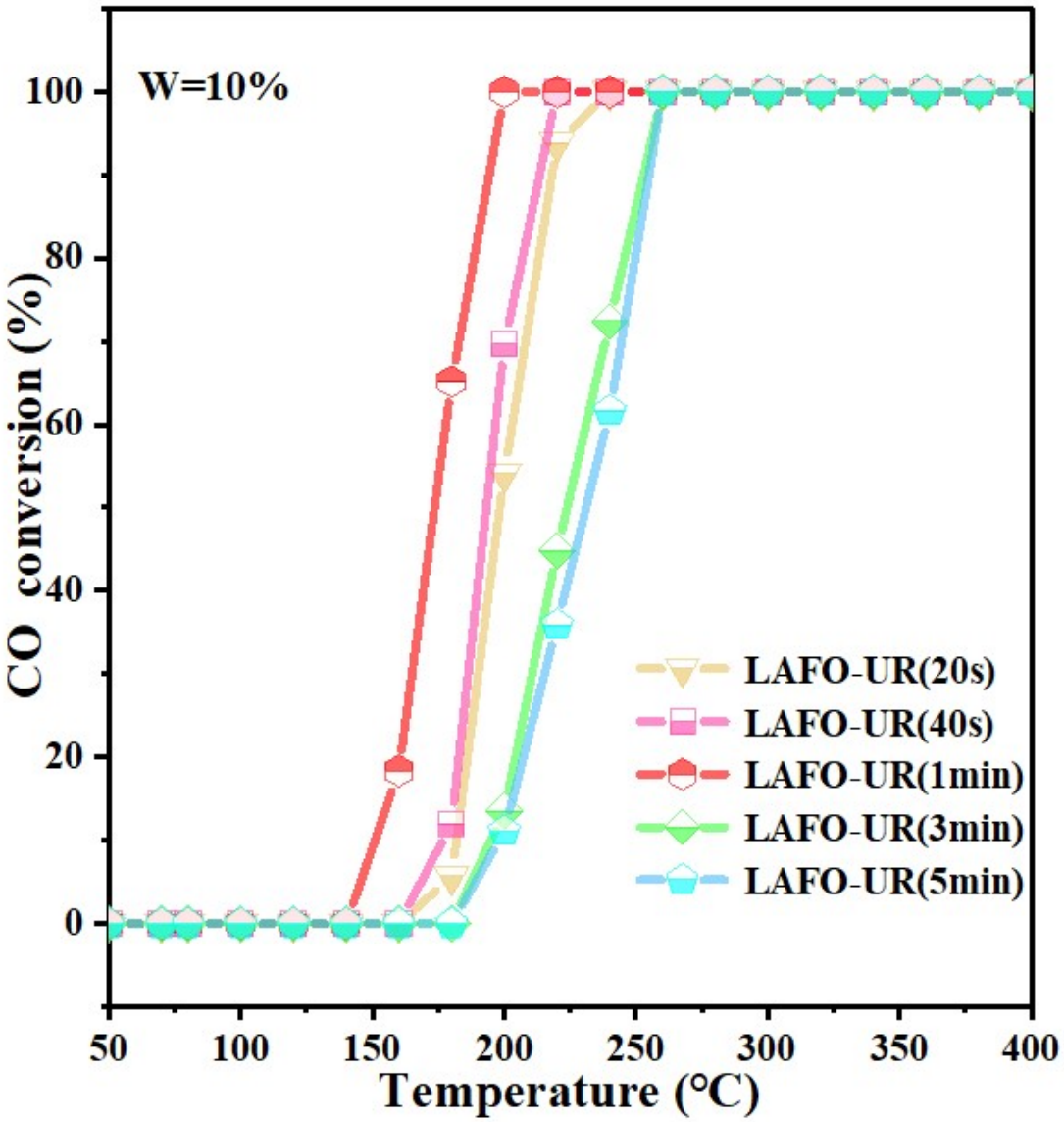

Figure S14. Light-off curves for CO oxidation of LAFO at different ultrasonic time.

The figure shows the CO catalytic oxidation capacity of LAFO at different ultrasonic time, LAFO catalytic capacity being the best at 1 min (W=10%).

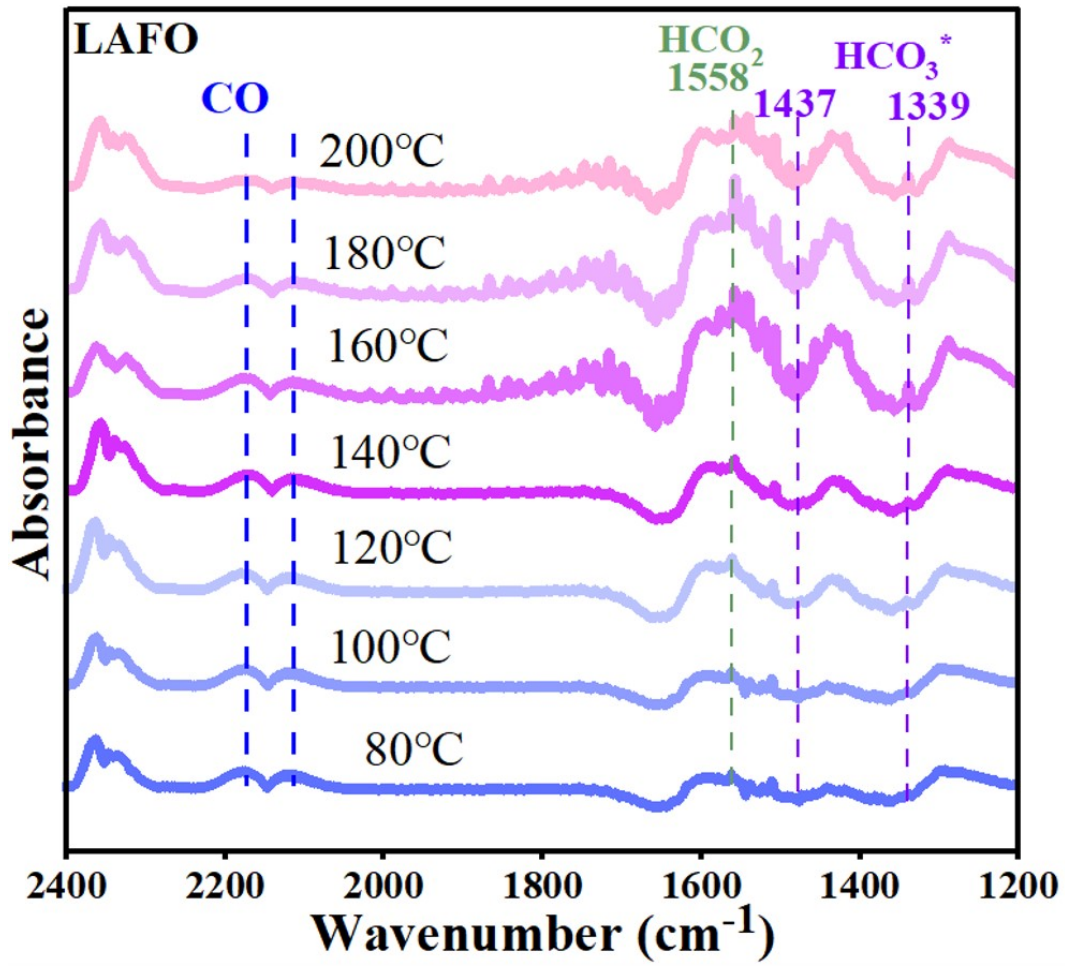

Figure S15. In situ DRIFTS spectra of LAFO in a reactive atmosphere(1%CO，20%O2/He).

The reaction path of LAFO is the same as that of LAFO-UR, the reaction mechanism is belongs to E-R mechanism.

Notes and refrences

[1] L. Yao, Z. Geng, W. Zhang, X. Wu, J. Liu, L. Li, X. Wang, X. Ke, K. Huang and S. Feng, *ACS Sustain. Chem. Eng.*, (2020),8, 17194-17200.

[2] Y. Cong, Q. Tang, X. Wang, M. Liu, J. Liu, Z. Geng, R. Cao, X. Zhang, W. Zhang, K. Huang and S. Feng, *ACS Catal*, (2019),9, 11743-11752.

[3] I. Martina, R. Wiesinger, D. Jembrih-Simbürger and M. Schreiner, *E-Preserv Sci*, (2012), 9, 1-8.